A review of melt extrusion additive manufacturing processes: I. Process design and modeling

Brian N. Turner, Robert Strong and Scott A. Gold
Chemical and Materials Engineering, University of Dayton, Dayton, Ohio, USA

Abstract

Purpose – The purpose of this paper is to systematically and critically review the literature related to process design and modeling of fused deposition modeling (FDM) and similar extrusion-based additive manufacturing (AM) or rapid prototyping processes.

Design/methodology/approach – A systematic review of the literature focusing on process design and mathematical process modeling was carried out.

Findings – FDM and similar processes are among the most widely used rapid prototyping processes with growing application in finished part manufacturing. Key elements of the typical processes, including the material feed mechanism, liquefier and print nozzle; the build surface and environment; and approaches to part finishing are described. Approaches to estimating the motor torque and power required to achieve a desired filament feed rate are presented. Models of required heat flux, shear on the melt and pressure drop in the liquefier are reviewed. On leaving the print nozzle, die swelling and bead cooling are considered. Approaches to modeling the spread of a deposited road of material and the bonding of polymer roads to one another are also reviewed.

Originality/value – To date, no other systematic review of process design and modeling research related to melt extrusion AM has been published. Understanding and improving process models will be key to improving system process controls, as well as enabling the development of advanced engineering material feedstocks for FDM processes.

Keywords FDM, Fused deposition modeling, Bead spreading, Liquefier dynamics, Melt extrusion manufacturing, Process modeling

Paper type Literature review

1. Introduction

Among the most widely used and rapidly growing rapid prototyping or additive manufacturing (AM) technologies are extrusion deposition processes such as fused deposition modeling (FDM®), fused filament fabrication and melt extrusion manufacturing (MEM) (Wohlers, 2011). In a typical process, a filament of material is fed into a machine via a pinch roller mechanism. The feedstock is melted in a heated liquefier with the solid portion of the filament acting as a piston to push the melt through a print nozzle. A gantry moves the print nozzle in the horizontal x–y plane as the material is deposited on a build surface that can be moved in the vertical z direction. This enables complex 3D objects to be produced as the melted bead leaving the nozzle solidifies. The most common materials used in this type of process are amorphous thermoplastics, with acrylonitrile butadiene styrene (ABS) being the most common. This article provides a more detailed overview of the typical components of extrusion-based AM processes and, more importantly, gives a review of the state of the art in process modeling and science for these processes.

The current issue and full text archive of this journal is available at **www.emeraldinsight.com/1355-2546.htm**

Rapid Prototyping Journal
20/3 (2014) 192–204
© Emerald Group Publishing Limited [ISSN 1355-2546]
[DOI 10.1108/RPJ-01-2013-0012]

1.1 Commercial market

Technologies first developed in the 1990s for rapid prototyping have grown in sophistication and their applications. Most parts produced with rapid prototyping in the past have been for use as visual aids, presentation models and rapidly produced, but not necessarily functional prototypes. While these applications remain a major part of the market for parts produced by melt extrusion AM and other 3D printing processes, a growing number of applications are for end-use parts that must meet stringent functional design requirements for mechanical properties and dimensional tolerances. The overall market for AM products and services has grown into a $1.325 billion industry (2010 estimate) and is projected to grow to over $5 billion by 2020 (Wohlers, 2011). AM machines can be found in a number of settings worldwide such as in industrial plants, homes/offices, service providers, academic institutions and government/military settings. Investments in AM research and development from both government agencies and the private sector have grown rapidly in recent years (Scott *et al.*, 2012), including the recent establishment of the National Additive Manufacturing Innovation Institute (NAMII, 2012).

Extrusion-based processes are among the most widely used AM technologies. The market for commercial extrusion-based AM systems is currently dominated by fused

Received: 30 January 2013
Revised: 12 March 2013
Accepted: 13 March 2013

deposition modeling (FDM) machines from Stratasys, Inc. According to the 2010 Wohler's Report, Stratasys' market share of industrial AM systems is 3.5 times that of any other system manufacturer at 41.5 per cent of all systems sold in 2010 (Wohlers, 2011). As of the end of 2010, there were > 15,000 Stratasys FDM machines installed worldwide (Wohlers, 2011). Their Fortus industrial manufacturing line of FDM systems cost $100,000-500,000 and are marketed to manufacture parts from engineering thermoplastic materials including Ultem® polyimide, polycarbonate and polyphenylsulfone, as well as ABS. Stratasys also produces widely sold, more economical Dimensions FDM systems that print only ABS thermoplastic materials, although in a variety of colors and grades. A Chinese company, Beijing Yinhua, has recently emerged as a competitor in this market with its MEM systems (Wohlers, 2011). Their E-Print and F-Print machines sell for $10,000-72,000 and are currently available in the Asian markets (Wohlers, 2011).

The rapidly growing personal fabrication market (Lipson and Kurman, 2010) is also dominated by fused filament fabrication-type systems, many of which are based on the open-source RepRap project (Jones *et al.*, 2011). The growth and popularity of these systems have been enabled by the expiration of the initial Stratasys patents on the FDM process, as well as the low cost and simplicity of construction of the systems. Among the more notable competitors in the personal and office use 3D printing market are the MakerBot® systems, the Bits-from-Bytes printers sold by 3D Systems, Inc. and the Up! Machines manufactured by Delta Micro Factory Corp. Stratasys is also a major player in this market with its Mojo® and uPrint® lines. Regardless of the manufacturer, these small-scale machines sell for $1,500-5,000 and print parts from ABS and/or polylactic acid (PLA) polymers.

1.2 Process modeling needs

Continued growth of the market for AM in general, but specifically for extrusion-based processes, is dependent on continued improvement in the performance and cost reduction of manufacturing systems, as well as the development of new feedstock materials. Process modeling can enable newly advanced model-based control systems and guide the development of new manufacturing hardware. Materials development will also be facilitated by improvements in our understanding of the processing science by placing bounds on acceptable feedstock properties (e.g. melt viscosity and filament elastic modulus) and expediting optimization of processing conditions. Furthermore, processing conditions play a major role in determining the properties of finished parts. Understanding these relationships will contribute to the development of design rules and quality control standards. An overview of key elements of an extrusion-based AM system will be presented. Modeling approaches and the current understanding of the processing science associated with each of these elements, namely, the pinch roller feed mechanism, liquefier, bead die swelling and cooling and road deposition and bonding, will be reviewed.

2. Overview of the design of the extrusion-based AM systems

Key elements of the melt extrusion AM system include a material feed mechanism, liquefier and print head, gantry, build surface and build environment. Components of a generic system are illustrated in Figure 1. The typical design features for each of these systems components are discussed in this section.

2.1 Material feed mechanism

Traditional extrusion manufacturing processes use a granular or pelletized feedstock with a screw-type extruder. While such a feed mechanism is theoretically feasible, to the best of our knowledge, no such mechanism is used in a commercially available AM system. Typical feedstocks are amorphous thermoplastic polymer filaments with a diameter of about 1.5-3 mm. In smaller-scale systems, this feedstock is simply a loose coil, while in larger manufacturing systems, the feedstock is coiled inside a cartridge to supply the system. In either case, the filament is pushed through the system using a pinch roller mechanism like that illustrated in Figure 1. A stepper motor is connected to one of the rollers providing energy to move the filament through the system. Typical roller materials are hypalon or polyurethane (Agarwala *et al.*, 1996). One or both of the rollers may have a grooved or toothed surface like a gear to create sufficient friction for the roller to grab the filament and feed it to the liquefier without slippage (Agarwala *et al.*, 1996). The pressure on the filament between the rollers is typically sufficient to slightly deform the filament, usually leaving small tooth marks, but these should be designed so as to avoid crushing the filament (Agarwala *et al.*, 1996).

Absorption of moisture by the polymer feedstock can present significant problems when printing parts in an extrusion-based process. As the material is melted and pushed through the extrusion nozzle, absorbed water vaporizes and, if present in sufficient quantities, can lead to morphological changes in the material, blockages (Halidi and Abdullah, 2012) of the print nozzle and/or formation of bubbles and bulges on the surface of the printed road of material. Stratasys,

Figure 1 Illustration of a typical extrusion-based AM process

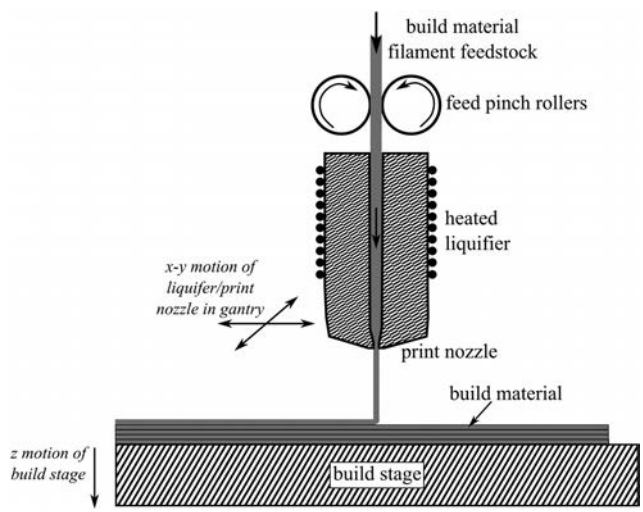

Inc. uses desiccant materials in both feedstock cartridges and in the FDM system itself to keep the build materials dry. Smaller systems typically do not have a mechanism to deal with this issue.

2.2 Liquefier, print head and gantry

At the heart of an extrusion-based AM system is the liquefier in which the polymer feedstock is melted. The liquefier is generally a metal block with a channel machined for the filament/melt to flow through. In Stratasys systems, the channel is connected to a disposable print head which is surrounded by the liquefier. Resistive heating is typically used with either a coiled heating element surrounding the liquefier chamber or one or more cartridge heaters embedded in the liquefier assembly. In either case, the system is designed to maintain a uniform temperature throughout the liquefier. A single thermocouple is used in conjunction with the heating element and a controller to maintain constant temperature (Gibson *et al.*, 2010).

Heat flux to the feedstock material must be sufficient to bring it to a melted state. The amount of melt in the liquefier will depend on the heat flux and the material feed rate. Feedstocks are generally amorphous polymers which do not have a distinct melting point. As the temperature increases, the viscosity of the melt decreases, allowing it to flow through the print nozzle more readily with a smaller pressure drop. Higher melt temperature also leads to better adhesion between successive beads or roads of printed material, and therefore greater mechanical strength in the finished part. Higher temperature can also lead to polymer degradation, breaking down polymer chains, weakening the finished part and leaving residue on the inside of the melt channel (Gibson *et al.*, 2010).

The print head is closely integrated with the liquefier and may be fixed or replaceable. The latter is generally preferable and is found on higher-end systems as thermal cycling and/or buildup of material residue will change the performance of the print head over time. The geometry of the print head along with the viscosity of the melt determines the pressure drop in the system and thus the force required from the material feed mechanism. The size of the print nozzle opening also places a limit on the resolution that may be achieved in a final printed product. Typical nozzle openings are about 200-500 μm in diameter.

The print head/liquefier assembly is attached to a gantry that enables motion in the x and y directions. Power to enable the motion is supplied by an electric stepper motor and transduced to the print head/liquefier through a gear and timing belt. The velocity at which the print head/liquefier can move, and ultimately the speed of part fabrication, is primarily limited by the stiffness of the construction of the gantry. The size of parts that can be printed is limited by the dimensions of the gantry.

2.3 Build surface and environment

Material is extruded from the print head/liquefier assembly onto a horizontal build surface which moves vertically (i.e. in the z direction). This motion, in conjunction with the print head motion in the gantry, allows 3D structures to be manufactured. The surface upon which the melt is printed is a critical element of the system design. The melt must adhere to this surface, but not so well that the part cannot be removed when the print process is complete. Stratasys machines utilize a disposable build sheet suitable for the build material which is placed on a vacuum-table build plate. Kapton™ films are among the more common build sheet surfaces used in open-source systems, which typically print only ABS and PLA polymers.

Thermal gradients are necessarily present in parts, as they are built in extrusion-based machines. Sufficiently large thermal gradients can lead to warping and distortion of the final structure (Wang *et al.*, 2007). Advanced systems print inside a temperature-controlled oven to combat this problem. Fans push air through the system to cool the parts as they are printed and to prevent buildup of heat radiating from the print head/liquefier in the build environment. This approach is necessary for high-melting polymers such as Ultem®. Smaller personal-scale and open-source systems use a heated build plate to reduce thermal gradients and part warping. This approach is cost-effective but limits the practical size of the build envelope and the melt temperature that can be used without thermal gradients becoming excessive.

2.4 Part finishing

A ridged surface is an inherent quality of parts produced from a melt extrusion AM process. The size of the ridges corresponds to the dimensions of the printed polymer roads extruded from the print nozzle. Two primary approaches are used to achieve smooth surfaces on parts: chemical and mechanical smoothing (Gibson *et al.*, 2010). Chemical smoothing systems expose the part to solvent vapors which are allowed to condense on the surface and partially melt it to smooth small ridges. Mechanical abrasion may also be used to smooth part surfaces, though this has limitations on parts with complex surface geometries due to inherent difficulties in abrasive materials entering small recesses, crevices or other features. Application of surface coatings is another approach to achieving a desired surface finish, in addition to adding strength to a finished part. Such coatings may include primers, paints or metallic electroplated coatings.

3. Process modeling and science

A major factor hindering the future growth of AM in general, and of extrusion-based processes in particular, is a limited understanding of processing science (Bourell *et al.*, 2009). Process models that describe the dynamics of the melt and extrusion process and the bonding process between successive layers of material are critical in developing advanced control strategies for AM systems. Understanding the relationships between process parameters and final part properties will be critical in enabling design of parts for manufacturing, in developing methods of qualifying parts for industrial use and in facilitating more intelligent materials development strategies. Key elements of an FDM or related process include the pinch roller feed mechanism, liquefier dynamics, road or bead spreading, bonding of adjacent roads of material to one another and shape changes due to thermal gradients within the part. The current state of the art in modeling each of these aspects of a typical process will be discussed in this section.

3.1 Pinch roller feed mechanism

A pinch roller mechanism is used to supply material to the liquefier in FDM-like processes. The filament feedstock is in tension above these rollers, which pull the filament from its source (Bellini *et al.*, 2004). Below the rollers, the filament is in compression, being pushed against the constricted opening of the print nozzle at the end of the liquefier (Bellini *et al.*, 2004). The feed rate is controlled so as to maintain a constant volumetric flow rate of material from the print nozzle, Q. For a desired road width (W) and slice thickness (H), the linear feed velocity of the filament (v) can be approximated as (Agarwala *et al.*, 1996; Bellini *et al.*, 2004):

$$v = \frac{Q}{WH} \tag{1}$$

The feed velocity can be most simply related to pinch roller parameters by assuming perfect adhesion between the filament and rollers, i.e. no slip. In this case, the feed velocity can be expressed as

$$v = \omega_r R_r \tag{2}$$

where ω_r is the angular velocity and R_r is the radius of the rollers, respectively (Bellini *et al.*, 2004; Agarwala *et al.*, 1996). A generalized Navier-slip boundary condition has also been applied. Sources of slip between the filament and rollers include mismatch between the roller surface material and filament surface, nonoptimal groove depth in the rollers, worn-out rollers or a sufficiently high-pressure drop in the liquefier such that the filament does not serve as an efficient piston (Agarwala *et al.*, 1996). Such slip leads to underflow of material from the liquefier nozzle and the impacts degree of bonding between adjacent roads (Agarwala *et al.*, 1996). Accounting for this slip has been found to be particularly important to accurately control the roller motor when sudden changes in the flow rate are made (Bellini *et al.*, 2004). The force necessary to push the melt through the liquefier can be determined if the pressure drop (ΔP) through the liquefier is known,

$$F = \Delta P A \tag{3}$$

where A is the cross-sectional area of the filament, assumed to be equal to the cross-sectional area of the liquefier (Bellini *et al.*, 2004). This in turn allows the required torque (Γ)

$$\Gamma = \frac{F}{2} R_r \tag{4}$$

and power (P_{mot}) to be calculated (Bellini *et al.*, 2004):

$$P_{mot} = \omega_r \Gamma \tag{5}$$

It is assumed that two motors are providing power to the roller mechanism in equation 5.

The compression on the liquefier side of the feed rollers places a limit on the feed rate. When this compression reaches a critical limit, the feedstock filament can buckle, as shown in Figure 2 (Venkataraman *et al.*, 1999, 2000a, b). This is the most common failure mode of the filament feedstock in extrusion AM processes with ceramic fillers (Venkataraman *et al.*, 2000b). An approximation of the critical pressure (P_{cr}) that can be placed on the filament can be obtained from an Euler buckling analysis,

Figure 2 Buckling of a filament between the feed pinch rollers and the liquifier entrance due to excess compression

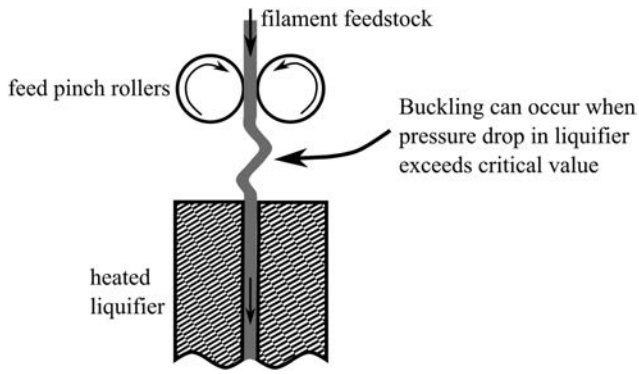

$$P_{cr} = \frac{\pi^2 E d_f^2}{16 L_f^2} \tag{6}$$

where E is the elastic modulus of the filament, d_f is the filament diameter and L_f is the filament length from the rollers to the entrance of the liquefier (Yardimci *et al.*, 1997; Venkataraman *et al.*, 2000b). Due to the difference between the filament diameter and the bore of the liquefier, a correction factor has been suggested for equation 6, allowing 1.1× the critical pressure for buckling to occur (Venkataraman *et al.*, 1999). In addition to placing limits on the feed rate, buckling also places bounds on the properties of the feedstock that can be used in an FDM process (Yardimci *et al.*, 1997; Venkataraman *et al.*, 2000b). By relating the critical pressure predicted by the Euler buckling analysis to the pressure drop in a capillary rheometer, Venkataraman *et al.* were able to estimate and experimentally validate that buckling did not occur above a critical value of the ratio of the elastic modulus of the solid feedstock to its apparent melt viscosity, E/η, of 3×10^5 to 5×10^5 s^{-1} (Venkataraman *et al.*, 2000b). Extension of this analysis in the future will aid in the development of composite feedstock materials for melt extrusion AM processes.

3.2 Liquefier dynamics

The liquefier and print head, where the solid polymer feedstock is melted and pushed through a small print nozzle, are the defining elements of extrusion-based AM processes. The dynamics of the liquefier are quite complex and challenging to model, as the melt properties are a nonlinear function of temperature and shear rate. The rate at which the filament is fed to the liquefier and ultimately printed is limited by the pressure drop through the nozzle. This feed rate is dynamically controlled, as the velocity at which the print head moves in the gantry of the system changes. The amount of melt present in the liquefier, the temperature of the melt and, consequently, the viscosity and surface energy of the melt vary with the feed rate. These variables control the rate at which the material flows through the liquefier and thus the size of the printed bead (i.e. resolution of the printed part). These melt

dynamics are critical in control algorithms for commercial systems. Furthermore, understanding these melt dynamics will help put bounds on the material properties necessary for a feedstock to be viable for commercial use. As will be discussed later, the temperature, viscosity and surface energy of the melt will have a major impact on the bonding of the printed polymer bead to neighboring beads.

3.2.1 Melt properties

The viscous behavior of the melt in the liquefier is critical in describing the behavior of the liquefier and extrusion nozzle. Feedstocks for extrusion AM processes are typically shear thinning and are commonly assumed to follow a power-law viscosity model (Bellini *et al.*, 2004; Mostafa *et al.*, 2009; Ramanath *et al.*, 2008; Yardimci *et al.*, 1997),

$$\eta = K(\dot{\gamma})^{n-1} \tag{7}$$

where η is the viscosity, $\dot{\gamma}$ is the shear rate and K and n are power-law fit parameters. The temperature dependence of viscosity must also be accounted for because the material will be nonisothermal as it flows through the liquefier chamber. This has been done by separating the viscosity into the product of a temperature and shear rate-dependent terms, respectively (Bellini *et al.*, 2004):

$$\eta = H(T)\eta_{T_0}(\dot{\gamma}) \tag{8}$$

The shear rate-dependent term is simply the power-law expression with fit parameters evaluated at some reference temperature, T_0. An Arrhenius model has been used for the temperature-dependent term,

$$H(T) = \exp\left[\alpha\left(\frac{1}{T} - \frac{1}{T_0}\right)\right] \tag{9}$$

where α is the activation energy (Bellini *et al.*, 2004; Karis *et al.*, 1996). Note that $H(T)$ is 1 at the reference temperature. To account for the material being solid at the entrance of the liquefier, the plug flow is assumed at the liquefier entrance.

To date, only power-law viscosity models have been used in published studies of FDM liquefiers. The primary advantage of the power-law model is its mathematical simplicity. It can be reasonably expected that some key aspects of the melt behavior will not be captured by this model. For example, no yield stress is included in the power-law model, which is characteristic of many polymer melts. Bingham-type models are widely used to describe the spreading of a printed bead of polymer material, as will be discussed later. The power-law model is also known to have difficulty accounting for wide ranges in the shear rate (Osswald and Menges, 2003). Relatively low shear is expected near the liquefier entrance, while very high shear is expected as the melt passes through the print nozzle. Shear rates in the nozzle are commonly in the range of 100-200 s^{-1} (Venkataraman *et al.*, 2000b). Carreau-type models are commonly used to account for both yield stress and wide ranges of shear rate in polymer melts, although with the addition of significant mathematical complexities (Osswald and Menges, 2003).

Modeling heat transfer in the liquefier is complicated by the temperature and shear dependence of the melt properties. It has been assumed that the heat capacity (c_p) of melt is constant in some models (Bellini *et al.*, 2004; Bellini, 2002). However, c_p is known to change significantly at the glass transition temperature (T_g) for amorphous polymers. As will be discussed later, temperatures above T_g are necessary to achieve good bonding between successively deposited layers of materials. While semi-crystalline polymers have not often been used in FDM-like processes, these typically introduce a greater change in the heat capacity on melting, as well as the need to account for the heat of melting/fusion for the material.

3.2.2 Liquefier/nozzle geometry

Besides the viscous behavior, the liquefier geometry has the greatest impact on the melt behavior in the liquefier. Most current systems use a straight cylindrical tube with a truncated conical connection to the small print nozzle opening, as illustrated in Figure 1. Older systems used a horizontal cylindrical tube that curved 90° before connecting to a liquefier geometry like that shown in Figure 1 (Ramanath *et al.*, 2008; Mostafa *et al.*, 2009). To facilitate modeling, the liquefier is typically divided into sections, as shown in Figure 3. Key design variables include the liquefier length (L_1), liquifier/filament diameter (D_1), nozzle angle (β), nozzle diameter (D_2) and nozzle length (L_2). Typical nozzle diameters are in the range of 200-500 μm, with nozzle angles typically at 120° (Yardimci *et al.*, 1997).

In either case, the diameter of the cylindrical entrance is typically assumed to be equal to the diameter of the feed filament. Clearly, the bore diameter must be somewhat larger to facilitate the insertion of the filament and to allow for a reasonable tolerance on the filament diameter. Any gap between the filament and the wall of the liquefier can be expected to lead to high thermal resistance to heat transfer from the liquefier walls to the filament. To date, this has not been accounted for in published models of FDM or related processes. This effect would be most significant at the top of zone I in Figure 3 and would diminish as material approaches the print nozzle and the compression force provided by the solid portion of the filament pushes the melt against the walls of the liquefier.

Figure 3 Liquifier divided into three zones for modeling

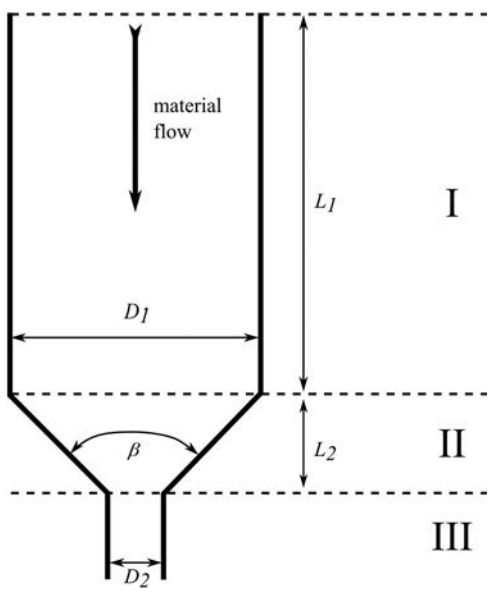

3.2.3 Estimation of heat flux

Analytical models of the liquefier have assumed either constant heat flux (Bellini *et al.*, 2004; Bellini, 2002) or constant wall temperature (Yardimci *et al.*, 1997; Ramanath *et al.*, 2008; Bellini, 2002). In the former case, an approximation of the required heat flux to the liquefier is given by the familiar equation,

$$q = \dot{m}c_p(T - T_i) = \left(\frac{\rho v A}{2\pi\left(\frac{D}{2}\right)L}\right)c_p(T - T_i) \qquad (10)$$

where $\dot{m}$ is the mass flow rate of the polymer through the liquefier, c_p is the heat capacity of the polymer and T and T_i are the temperatures of the polymer at the exit and entrance of the liquefier, respectively. Typically, the feed velocity will be controlled rather than the mass flow rate; therefore, it is convenient to approximate the mass flow rate in terms of this velocity (v), the polymer density (ρ) and the liquefier dimensions (length, L; cross-sectional area, A; and diameter, D). The high thermal conductivity of the liquefier, typically constructed of aluminum, steel or brass, has led others to postulate a constant wall temperature in the liquefier (Yardimci *et al.*, 1997; Ramanath *et al.*, 2008). The accuracy of either assumption rests, in part, on the design of the liquefier. The most common designs use either a resistive heating element coiled around the liquefier or a cartridge heater embedded in the metal parallel to the liquefier chamber. The design of the latter requires some mechanism to evenly distribute heat to all sides of the liquefier chamber, such as drilling insulating holes between the heater and liquefier chamber as in some Stratasys systems. Some degree of nonuniformity is expected, especially in an unsteady-state operation. Only a single thermocouple embedded in the liquefier is typically used to control the melt temperature.

3.2.4 Convection at the liquefier entrance and nozzle exit

Finite element analysis (FEA) has been used to examine temperature gradients within the liquefier (Yardimci *et al.*, 1997). This analysis examined heat convection to the build environment at the liquefier entrance and at the nozzle exit, assuming a convective heat transfer coefficient (h) of 10 W/m^{2}K at the entrance and 100 W/m^{2}K at the nozzle exit (Yardimci *et al.*, 1997). These values of h were not justified by any experimental or theoretical analysis, and heat loss from the liquefier is not surprisingly highly sensitive to values chosen. In real systems, it is typical to include an insulating plate at both locations to prevent heat loss, a practice that appears to be well justified based on FEA and the selected values of h (Yardimci *et al.*, 1997).

3.2.5 Location of the melt front

Filament heating has been described by a two-dimensional (2D) axisymmetric steady-state advection-conduction model, assuming a constant wall temperature and plug flow (Yardimci *et al.*, 1997). The nondimensional solution to this problem is given as:

$$\theta = 2\sum_{n=1}^{\infty}\exp(-\lambda_n^2 z')\frac{\mathcal{J}_0(\lambda_n r')}{\lambda_n \mathcal{J}_1(\lambda_n)},\ \mathcal{J}_0(\lambda_n) = 0 \qquad (11)$$

where θ, r' and z' are the dimensionless temperature, radius and length respectively, defined as

$$\theta = \frac{T - T_0}{T_2 - T_0},\ r' = \frac{r}{r_f},\ \text{and}\ z' = \frac{\alpha z}{v r_f^2} \qquad (12)$$

T is the filament temperature at some point (r, z), T_0 is the wall temperature, T_2 is the temperature of the filament at the entrance of the liquefier ($z = 0$), r_f is the filament radius, α is the thermal diffusivity of the filament, v is the filament velocity, λ_n are roots of the zero-order Bessel function of the first kind ($\mathcal{J}_0$) and $\mathcal{J}_1$ is the first-order Bessel function of the first kind. This solution assumes constant thermal properties of the filament and neglects any gap between the filament and the liquefier wall. Solving for z' when $r' = 0$ and $T = T_m$, that is when the temperature of the center of the filament is equal to the melt temperature, allows the location of the melt front to be calculated (Yardimci *et al.*, 1997). The distance from the entrance to the melt front increases linearly with the filament velocity, which is dynamically varied in commercial melt extrusion AM systems (Yardimci *et al.*, 1997). The distance from the entrance to the melt front increases linearly with the filament velocity, which is dynamically varied in commercial melt extrusion AM systems. The filament velocity and heat flux to the liquefier must thus be set at values to maintain the melt front somewhere in the middle of the liquefier length. The melt front distance is also inversely proportional to the thermal diffusivity of the material, highlighting the challenges of processing highly thermally insulating materials in extrusion AM processes.

3.2.6 Pressure drop estimation

From a momentum balance on the liquefier, the melt velocity profile, pressure drop and shear stress profile can be predicted. When solved simultaneously with an energy balance, the temperature profile of the melt within the liquefier can be determined (Bellini *et al.*, 2004; Bellini, 2002) and others, building on their work (Ramanath *et al.*, 2008) used analytical solutions to the momentum balance equations developed for extrusion dies (Michaeli, 2003) for cylindrical, conical and cylindrical shapes corresponding to regions I, II and III, respectively, in Figure 3 in conjunction with a power-law viscosity model with Arrhenius temperature dependence (cf. equations 7 and 8) to model the liquefier. Key assumptions in this model include that the melt is incompressible, a no-slip boundary condition applies at the walls of the liquefier and that the flow is fully developed, steady state and laminar (Michaeli, 2003). The pressure drops in each section of the liquefier according to this model are given respectively by:

$$\Delta P_1 = 2L_1\left(\frac{v}{\phi}\right)^{1/m}\left(\frac{m+3}{(D_1/2)^{m+1}}\right)^{1/m}\exp\left[\alpha\left(\frac{1}{T} - \frac{1}{T_\alpha}\right)\right] \qquad (13)$$

$$\Delta P_2 = \left(\frac{2m}{3\tan(\beta/2)}\right)\left(\frac{1}{D_2^{3/m}} - \frac{1}{D_1^{3/m}}\right) \times \left(\left(\frac{D_1}{2}\right)^2 (m+3)2^{m+3}\right)^{1/m} \times \exp\left[\alpha\left(\frac{1}{T} - \frac{1}{T_\alpha}\right)\right] \qquad (14)$$

and

$$\Delta P_3 = 2L_3\left(\frac{v}{\phi}\right)^{1/m}\left(\frac{(m+3)(D_1/2)^2}{(D_2/2)^{m+3}}\right)^{1/m}\exp\left[\alpha\left(\frac{1}{T}-\frac{1}{T_\alpha}\right)\right] \quad (15)$$

where the dimensions L_1, L_3, D_1 and D_2 correspond to Figure 3, β is the nozzle angle of the conical section of the liquefier, and m and φ are power-law fit parameters (Ramanath *et al.*, 2008; Bellini *et al.*, 2004; Bellini, 2002; Michaeli, 2003). The total pressure drop in the liquefier is the sum of the pressure drops in each section,

$$\Delta P = \Delta P_1 + \Delta P_2 + \Delta P_3 \quad (16)$$

3.2.7 Impact of nozzle angle

The nozzle angle, typically 120° in most systems (Yardimci *et al.*, 1997), will influence the pressure drop and flow characteristics in a system. Ramanth *et al.* examined the impact of nozzle angle on pressure drop for angles up to 60°, showing that pressure drop decreases with increasing nozzle angle (Ramanath *et al.*, 2008; Bellini *et al.*, 2004); however, 120° is a typical nozzle angle (Yardimci *et al.*, 1997). Above the natural convergence angle for the system, the pressure drop can increase due to flow instabilities and vortices that may form in the corner of the die (Liang, 1995; Liang *et al.*, 2001; Liang and Ness, 1997), which may also lead to clogging of the nozzle when using filled feedstocks (Yardimci *et al.*, 1997). The natural convergence angle has been suggested as an upper bound for designs of the nozzle angle (Yardimci *et al.*, 1997). The critical pressure for buckling (cf. equations 6, 13-16) places a lower limit on the nozzle angle design.

3.2.8 Finite element analyses

More rigorous analyses of the melt fluid dynamics and liquefier heat transfer have been achieved through FEA (Ramanath *et al.*, 2008; Mostafa *et al.*, 2009; Ji and Zhou, 2010; Bellini *et al.*, 2004). Pressure drop predictions from FEA analyses agree qualitatively with the analytical model described in equations 13-16, showing an increased pressure drop as the nozzle diameter decreases or as the feed velocity increases (Ramanath *et al.*, 2008; Bellini, 2002; Bellini *et al.*, 2004). Quantitatively, the FEA models predict significantly lower pressure drop ($\sim 5 \times 10^5$ Pa) than the analytical model summarized in equations 13-16 (Ramanath *et al.*, 2008). This difference is most likely due to the more stringent assumptions made in deriving the analytical model to make it mathematically tractable (Michaeli, 2003). FEA analyses indicate that the overwhelming majority (approximately 85 per cent) of the pressure drop in the liquefier occurs in the vicinity of the nozzle (Venkataraman *et al.*, 2000a; Bellini, 2002), along with a strong dependence on the nozzle diameter. In a study of poly-ε-caprolactone, increasing nozzle size from 0.25 to 0.4 mm reduced the calculated pressure drop from $\sim 2.5 \times 10^6$ to $\sim 1 \times 10^6$ Pa.

While FEA models predict rapid temperature changes at the liquefier entrance and nozzle exit, the small size of filament allows nearly uniform temperature in the melt to be achieved quickly with variations from wall to centerline of often < 1 K (Bellini, 2002; Bellini *et al.*, 2004; Mostafa *et al.*, 2009; Ramanath *et al.*, 2008). Similarly, a parabolic velocity profile is predicted to develop rapidly after the melt front is established (Bellini, 2002; Bellini *et al.*, 2004; Mostafa *et al.*, 2009; Ramanath *et al.*, 2008). Laminar flow pathlines are also predicted (Bellini, 2002; Bellini *et al.*, 2004; Mostafa *et al.*, 2009; Ramanath *et al.*, 2008), but no evidence of flow instabilities and vortices due to the nozzle angle being above the natural convergence angle has been reported.

3.3 Die swelling and bead cooling

In the nozzle, the polymer melt is under stress, with part of the deformation energy being stored elastically (Michaeli, 2003). As the polymer melt leaves the print nozzle, the now free boundary of the polymer melt allows the polymer bead to quickly assume a plug-flow velocity profile, i.e. constant velocity in the radial direction (Bellini, 2002). With the polymer melt no longer constrained by the walls of the liquefier, stresses that were acting on the melt in the nozzle are relaxed and the elastically stored energy is released, leading to radial expansion of the melt referred to as die swelling, as illustrated in Figure 4 (Michaeli, 2003). The phenomenon is an active area of polymer rheology research and plays a role in determining the resolution achieved in an extrusion-based AM process. A quantitative measure of die swelling is the ratio of the maximum diameter of the extruded material to the diameter of the die opening, referred to as the swelling ratio, s. The value of the swelling ratio depends on the material properties and the geometry of the extrusion nozzle. Reported values for FDM-like processes ranged from $\sim$ 1.05 to 1.3. Inelastic fillers such as ceramic particles (Bellini, 2002) or carbon fibers (Shofner *et al.*, 2003) tend to reduce die swelling. FEA models have been used to predict die swelling for FDM-like processes (Bellini, 2002) and other extrusion processes.

As the melt leaves the extrusion nozzle, it is also subject to convective cooling from air moving in the build environment. Bellini modeled this convective cooling assuming a heat transfer coefficient, $h = 20$ W/m^{2}K (Bellini, 2002). The convective cooling process is retarded by heat conduction from the melt in the liquefier still connected to the extruded bead (Bellini, 2002). Somewhat counterintuitively, the greater the thermal conductivity of the melt, the slower the bead will cool on leaving the extrusion nozzle (Bellini, 2002).

3.4 Road deposition, spreading and bonding

3.4.1 Bead deposition and stability

After leaving the liquefier nozzle in a melt extrusion AM process, a bead of polymer melt ultimately lands on a build

Figure 4 Illustration of die swelling in an extrusion AM process

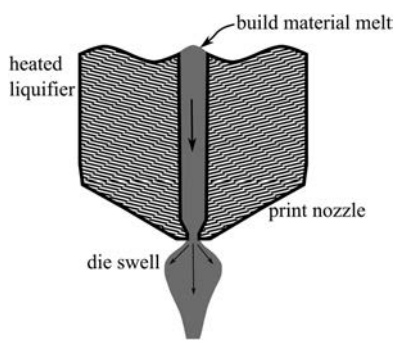

sheet or on a previously printed bead of polymer. If flow through the print nozzle, region III in Figure 3, is modeled as a simple Hagen-Poiseuille flow, the volumetric flow rate, Q, is (Crockett and Calvert, 1996):

$$Q = \frac{\pi\left(\frac{D_2}{2}\right)^4 \Delta P}{8\eta L_2} \tag{17}$$

The cross-sectional area (A) of the bead will be inversely proportional to the velocity of the print head (v_{print}).

$$A = \frac{Q}{v_{print}} \tag{18}$$

If the print head velocity is sufficiently large, the bead will become unstable and discontinuous. As the maximum velocity for which the bead remains stable and continuous is approached, the deposition has been described as similar to an axisymmetric liquid bridge, allowing the maximum velocity of the print head to be estimated (Crockett, 1997; Crockett and Calvert, 1996; Middleman, 1995),

$$v_{print} < \frac{Q\pi}{h^2} \tag{19}$$

as well as the minimum cross-sectional area (Crockett, 1997; Crockett and Calvert, 1996; Middleman, 1995),

$$A_{min} = \frac{h^2}{\pi} \tag{20}$$

Here, h is the height of the print nozzle opening above the print surface.

3.4.2 Road spreading

The bead or road will spread into an oblong shape with the spreading rate and final shape dependent on the viscosity of the melt and the relative surface energies of the bead and the surface on which it is printed. The interaction of the tip of the print head with the bead may further influence the evolution of the shape of the printed road. As it spreads, the bead is also cooling, and the viscosity increases until a solid state is reached. The final width of the road determines the resolution that can be achieved in the print process, as well as the contact area between neighboring beads. The rounded, oblong shape of the bead inevitably leads to small voids in the part. The strength of the bond between neighboring roads, and ultimately the overall mechanical properties of the part, will depend on the contact area between those beads and the size of the voids.

While there is a wealth of literature on the spreading of liquid droplets on a surface, only a limited number of efforts to model the bead spreading in an AM process have been published. Crockett *et al.* approximated the bead-spreading process as a laminar axisymmetric flow (Middleman, 1995), assuming a constant bead cross-sectional area (i.e. no shrinkage) and a Bingham viscosity model (Crockett, 1997; Crockett and Calvert, 1996). Only surface tension forces, which were assumed to be constant, were accounted for in the model (Crockett, 1997; Crockett and Calvert, 1996). The influence of gravity and any initial velocity profile in the bead was neglected. While the influence of the tip nozzle was not explicitly taken into account, two boundary conditions on the top surface of the bead were explored, a free surface where

$$\left(\frac{\Delta W}{\Delta t}\right)_{x=W} = \frac{A}{8\eta W^2}\left(\frac{F(\theta)}{l} - 2\tau_y(t)W\right) \tag{21}$$

and a constrained surface where the right side of the above equation is multiplied by a factor of 1/4 (Crockett, 1997). Here $F(0)/l$ is the driving force for spreading per unit length of the bead, τ_Y is the yield strength of the liquid bead and W is the bead width. Similarly, the change in contact angle was described as

$$\left(\frac{\Delta\phi}{\Delta t}\right)_{x=R\phi} = \frac{A\gamma_{LV}}{8\phi R^3\eta}\left(\frac{\cos\phi - \cos(\theta - \phi)}{\phi} - \frac{2\tau_Y(t)R}{\gamma_{LV}}\right) \tag{22}$$

for the free surface boundary condition with the right side of the equation multiplied by a factor of 1/4 for the constrained surface boundary condition. Here φ and θ are the contact angles of the bead as illustrated in Figure 5, assuming the bead is printed on a surface with a circular cross-section. While the free surface boundary condition seems more intuitive, the constrained surface boundary condition was reported to show greater agreement with an experiment with a ceramic slurry, although still consistently a predicted bead width of approximately 25 per cent greater than the experimental and final contact angles of approximately 35 per cent less than observed (Crockett, 1997). These reported results are somewhat misleading, as perfect wetting was also assumed in this model. As a result, if the model is evaluated for sufficiently long times, the bead will spread to completely wet the surface it is being printed on. The complete wetting assumption was justified in that for 3D structures, printing of some material on a self-similar material will result in complete wetting, as the bead and substrate will have the same surface energies. Even in this case, some small differences would be expected because the substrate will be a solidified material rather than a melt. Incorporation of a term accounting for the cooling and temperature dependence of viscosity would correct for this problem. While Crockett's model has not been evaluated for a polymer melt and does have major drawbacks, it should, however, provide a useful framework for describing the spreading behavior of such materials in an FDM-like process.

Figure 5 Illustration of road spreading and the force balance used in the Crockett model

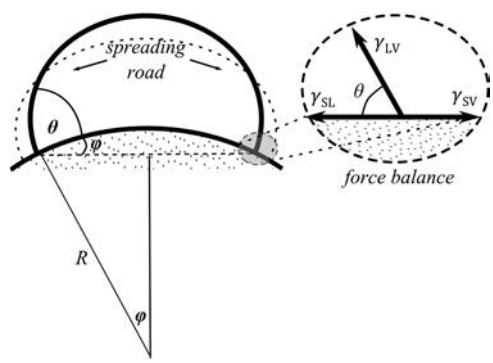

Frenkel-type models based on an energy balance (Frenkel, 1945) have been widely used to describe spreading of liquids (Crockett, 1997; Park, 2003; Duineveld, 2003; Mao, 1997). The change in the energy of the droplet due to a product of surface energy and change in the surface area and viscous dissipation is used to predict the change in the shape of the drop over time. This approach should yield an equivalent result to a momentum balance approach used by Crocket, and indeed found it to be so (Karis *et al.*, 1996). The initial kinetic energy of the bead from the deposition process was, however, neglected.

A 2D simulation of the bead-spreading process using commercial computational fluid dynamics (CFD) software was presented by Bellini for an FDM process (Bellini, 2002). In setting up the model, a no-slip boundary condition between the melt and the wall of the print nozzle was assumed along with a constant nozzle wall temperature. The free surface of the road was assumed to have a constant surface tension and to be losing heat due to convection from the air in the build environment as well as conduction to the surface below. Simulations accounting for the interaction of the print nozzle with the printed road, as shown in Figure 6, as well as with the print nozzle above the printed road were performed. The nozzle was shown to be beneficial, resulting in more stable flow and ensuring a flat road surface, as shown in Figure 6. It was also shown that the rate of convective heat loss plays a large role in the evolution of the road temperature. Distortion of the road in simulations when the print head was above the road surface can be speculated to be due to an effect similar to that seen in die swelling.

3.4.3 Road cooling and polymer bonding

The strength of a melt extrusion AM part will be limited fundamentally by the strength of the bond between neighboring beads of material in the part. This bond strength will be a function of the energy of adhesion/cohesion, which will depend in part on the contact area between the beads. For polymer materials, road bonding occurs through a sintering process which transpires through a viscous flow mechanism (Rosenzweig and Narkis, 1981). As this sintering process is thermally driven, the temperature history of a road at the interface with another road will be a crucial variable in determining the quality of the bond. A prerequisite to the sintering process is that the polymer be above the glass transition temperature, T_g. On leaving the liquefier, the melt is well above this temperature; however, the build environment is held well below T_g. Heat from the material leaving the liquefier increases the temperature of the road it is deposited on above T_g to enable bonding. Consequently, the thermal conductivity and heat capacity of the materials play a key role in determining viable process operating conditions. Heat is lost from the roads via conduction to the material below and convection to the surrounding air in the build environment.

Several models have been developed to predict the thermal history of a road. Thomas and Rodriguez presented a simplified 2D thermal model that treated the roads as rectangular in shape (Thomas and Rodriguez, 2000). The resulting equation for the filament temperature averaged over the width of the road for filament height, H, and width, W, is:

$$T_{ave}(x,y,t) = T_E\left[1 + \sum_{m=1}^{\infty}\sum_{n=1}^{\infty}(a_{mn}\sin(\lambda_m y)\cos(\beta_n x)) \times exp\left(-\left(\frac{k}{C\rho}\right)^2(\lambda_m^2 + \beta_m^2)t\right)\right] \quad (23)$$

where

$$a_{mn} = \frac{4T_L^*}{E_m^2 F_n^2 \lambda_m \beta_n}\sin\left(\frac{9\lambda_m H}{2}\right)\sin\left(\frac{\lambda_m H}{2}\right)\sin\left(\frac{\beta_n W}{2}\right) \quad (24)$$

$$E_m^2 = \frac{1}{2}\left(5H - \frac{\sin(10\lambda_m H)}{2\lambda_m}\right) \quad (25)$$

$$F_n^2 = \frac{1}{2}\left(\omega - \frac{\sin(\lambda_n \beta_n W)}{\beta_n}\right) \quad (26)$$

Here, t, C, k and ρ are time, heat capacity, thermal conductivity and density, respectively, and the eigenvalues are the roots of the equations (Thomas and Rodriguez, 2000):

$$\lambda_m \cot(5\lambda_m H) = -\frac{h}{k} \quad (27)$$

and

$$\beta_n \tan\left(\frac{\beta_n W}{2}\right) = \frac{h}{k} \quad (28)$$

This model neglected the effects of conduction to the build surface and any contact resistances between filaments, the former of which is the predominant heat transfer mechanism in the system (Bellehumeur *et al.*, 2004). Observing that the 2D analysis showed temperature gradients that rapidly become negligible along the width and height of the filament led Belleheumer *et al.* to propose a lumped capacity model which

Figure 6 Interaction of the print head with an extruded road

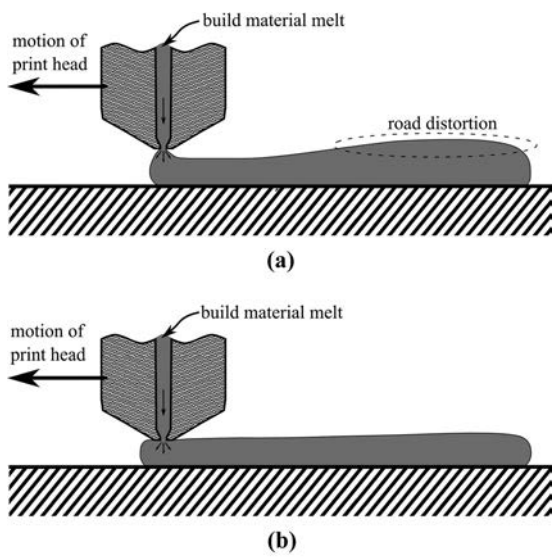

Notes: (a) The road shape is distorted when the print head is above the deposited road. (b) the print head in contact with the road helps ensure a flat top road surface

assumed uniform temperature distribution of cross-sectional area of filament, semi-infinite filament length and constant heat transfer and convection coefficients (Bellehumeur *et al.*, 2004; Sun *et al.*, 2008). This simplified the governing equations to a 1D transient heat transfer equation,

$$\rho CAv\frac{\partial T}{\partial x} = A\frac{\partial\left(k\frac{\partial T}{\partial x}\right)}{\partial x} - hP(T - T_\infty) \quad (29)$$

the analytical solution of which is:

$$T = T_\infty + (T_0 + T_\infty)\exp\left(\frac{(1 - \sqrt{1 + 4\alpha\beta})vt}{2\alpha}\right) \quad (30)$$

$$\alpha = \frac{k}{\rho C_v}, \text{ and } \beta = \frac{hP}{\rho CAv} \quad (31)$$

This approach has the advantage of simplicity but does not allow any special resolution of the temperature within the road to be predicted. While the 2D model predicts a rapid initial drop in temperature (for times < 1.5 seconds) when a new road is deposited, the lumped capacity model predicts a steady drop in temperature over time. A commercial CFD package has also been used to model the thermal history of a road as has been discussed earlier (Bellini, 2002).

Experimental validation of models was accomplished by embedding a thermocouple in a material road on the build surface and monitoring the temperature as successive layers are deposited on top of it (Bellini, 2002; Bellehumeur *et al.*, 2004; Sun *et al.*, 2008). At short times where the temperature was highest, the lumped capacity model showed better agreement with the experiment, whereas the 2D model proved to be more accurate at longer times and lower temperatures. No experimental comparison with predictions made by commercial CFD software has been published, although such a model for a fused deposition of ceramics process was shown to be very accurate, except at very short times (< 0.03 seconds) (Bellini, 2002). Qualitatively, experiments showed that the temperature of a road increases almost instantaneously when a melt layer is deposited on top of it followed by a rapid decay, on a time scale of $\sim$ 2s, back below the glass transition temperature to a few degrees above the build environment temperature (Sun *et al.*, 2008). The temperature in the bottom layer did not return to the equilibrium build environment temperature even after as many as 30 layers were deposited (Sun *et al.*, 2008). Given the small size of the test structure being evaluated, it is possible that radiative heating by the print head itself left the local environment temperature higher than that of the bulk of the build environment, preventing further cooling. As successive depositions can raise the material temperature above T_g, even several layers down, the time between successive depositions is also important in determining the thermal history of the material. This was demonstrated for two different part orientations with differing toolpath lengths (Sun *et al.*, 2008).

A consequence of these observations is that the dependence of the mechanical properties of a given part on toolpaths and part orientation is far more complex than it may appear at first glance. It is well established that the mechanical properties of an FDM® part are anisotropic with the greater tensile strength in the axial direction of a road than in the transverse direction, normal to road-to-road bonds (Ahn *et al.*, 2002). Reducing the time between the depositions of successive layers over a given point should also increase bond strength as the temperature at the bonding site would stay higher for a longer period of time. Specimens fabricated using a "level domain decomposition" which reduced the average road length compared to standard unidirectional raster patterns seem to validate this idea (Bellini and Guceri, 2003).

The thermal history of a bead was observed to be highly dependent on convective cooling by air flowing through the build environment (Sun *et al.*, 2008). Values of the convective heat transfer coefficient have been approximated to be around 20 W/m^{2}K (Bellini, 2002), although no empirical measurements validating this choice have been reported. The value of the heat transfer coefficient is expected to vary with the location in the build environment and air flow rate, as well the size, shape, number and distribution of parts within the build environment (Sun *et al.*, 2008). Experimental validation of convective heat transfer in an FDM® process presents a challenging problem, as air flow rates and build environment temperatures are not readily controllable in typical commercial systems. Rigorous computational analysis of convective heat transfer is likely to be of limited value due to the computational intensity of the problem; however, establishing some extreme bounds on the process would be of great use in developing process and product design rules.

While there have been numerous empirical studies of the impact of process parameters on the strength of the final part, little has been published examining the fundamental relationship between the bond formation process and the final mechanical strength of that bond. A figure of merit that has been used in evaluating the bonding process between adjacent roads is neck formation (Bellehumeur *et al.*, 2004; Sun *et al.*, 2008). This process occurs through viscous flow and molecular diffusion of polymer chains across the interface between two particles of beads until they are randomized, as illustrated for filaments of radius a and neck length $2y$ in Figure 7. A modified Frenkel sintering model based on

Figure 7 Illustration of polymer sintering

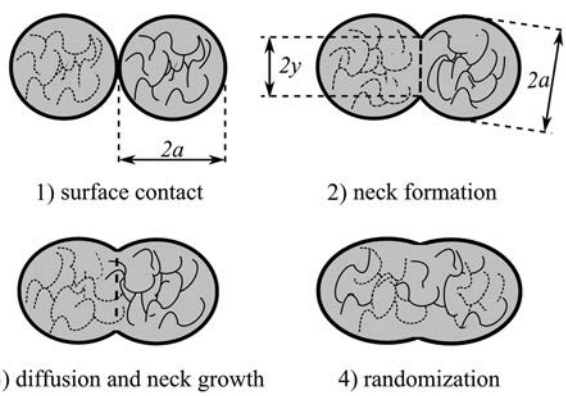

Notes: 1) initial contact between roads of radius *a*. 2) neck formation. 3) inter-diffusion of polymer chains and neck growth and 4) randomization of polymer chains between adjacent roads. Neck length, 2*y*, provides a measure of bond quality

Newtonian sintering has been used (Bellehumeur *et al.*, 2004; Sun *et al.*, 2008) to predict neck growth in terms of a dimensionless parameter $\theta = \sin^{-1}(y/a)$ with respect to time as a function of the viscosity (η), surface tension (Γ) and the initial particle radius, a_0:

$$\frac{d\theta}{dt} = \frac{\Gamma}{a_0\eta}\frac{2^{-5/3}\cos\theta\sin\theta(1-\cos\theta)^{1/3}}{(1-\cos\theta)(1+\cos\theta)^{1/3}} \quad (32)$$

In this analysis, surface tension was used as a fit parameter, rather than from the experimental data. Below some critical sintering temperature, no significant neck formation is observed. This temperature is well above the glass transition temperature, 200°C for ABS compared to T_g of 94°C (Bellehumeur *et al.*, 2004). A significant degree of molecular diffusion is expected to occur between these temperatures that will not be accounted for in measurements of neck formation. Nonetheless, neck formation is expected to show a strong correlation with bond strength.

4. Summary and conclusions

At least first-generation models have been developed for all major aspects of melt extrusion AM processes. There remains much room for improvement. In general, there has been a limited degree of experimental validation of process models. For example, simple models allow estimation of the required motor torque and power to achieve a desired filament feed rate for the commonly used pinch roller feed mechanism, as well as the impact of variations in the feed filament diameter on the flow rate leaving the extrusion nozzle (Bellini *et al.*, 2004; Agarwala *et al.*, 1996). These models are sufficient for sizing of motors in the system design and for providing a good qualitative understanding of the process. Slip between the pinch rollers and feed filament has been accounted for to some degree in these models; however, it has not been experimentally measured in the published literature. The degree of slip should be a function of the roller and feedstock material surface characteristics and the pressure exerted by the rollers. Minimizing slip without crushing the filament presents an interesting system design problem. More important is accounting for this slip in a closed-loop control algorithm. Some guidance in an approach to doing this has been provided in terms of both an analytical model as well as when using a transfer function approach (Bellini *et al.*, 2004), although the accuracy of these models was not experimentally evaluated.

Buckling failure of the feed filament between the pinch rollers and liquifier places a limitation on acceptable feedstock properties and operating conditions. Mathematically, this failure mode was modeled using an Euler buckling analysis with the critical pressure for buckling being a function of the filament diameter, its elastic modulus and the distance from the pinch rollers to the liquifier entrance (Yardimci *et al.*, 1997; Venkataraman *et al.*, 2000b). The difference between the liquifier bore diameter and the filament diameter was not accounted for theoretically, but it has been incorporated into the model through an empirical correction factor (Venkataraman *et al.*, 1999). While this does leave some room for improving the model theoretically, the practical value of doing so would be somewhat limited. The key value of the buckling analysis is to place some practical bounds on acceptable feedstock properties and pressure drop in the liquifier. Buckling is not generally a problem with amorphous polymer feedstocks most commonly used in FDM® and similar processes. However, this would not be expected to be the case for highly filled feed filaments such as those used for fused deposition of ceramics and metals, and chopped fiber-filled thermoplastic composite feedstocks, as these generally have a higher elastic modulus as well as higher melt viscosity. The key value of this buckling analysis is in providing qualitative guidance to material development (e.g. when addition of a plasticizer might be needed) and determining a maximum pressure drop and hence flow rate from the print nozzle in a given system.

Models of liquifier dynamics were reviewed previously. Understanding liquifier behavior is critical in melt extrusion AM systems as a dynamic control is required to change the feed rate with print head velocity to maintain a constant road width and ensure that the printed bead has sufficient thermal energy to form a strong bond with the material on which it is printed. One of the first challenges in modeling liquifier behavior is the complex behavior of the melt, with viscosity having both temperature and shear rate dependence. Generally, viscosity in the liquifier has been described by a power-law model for the shear dependence in combination with an Arrhenius-type temperature dependence expression. While this approach to modeling polymer melt viscosity is common, it presents two challenges. First, there is a need for published viscosity data for commercial feedstocks. As with other polymer-processing technologies, commercial feedstock filaments are optimized for the process. The overwhelming majority of modeling studies on melt extrusion AM processes have focused on ABS, which is the most commonly used polymer for these processes. To the authors' knowledge, there are no published reports of the viscosity behavior of other commercially available feed materials for melt extrusion AM processes. It is expected that this need will be even more acute for polymers with increasing degrees of crystallinity and thus more dramatic transitions in material properties from the solid to the melt phase. A second challenge in modeling viscosity behavior occurs not in modeling the spreading of a printed road. An important characteristic of the printed road is its yield stress, which must be sufficient for the road to not deform when successive roads are printed atop it. Measurements of yield stress are almost nonexistent for commercial feedstock materials used in melt extrusion AM processes.

Heat transfer in the liquifier has been modeled analytically with the assumption of either constant heat flux (Bellini *et al.*, 2004; Bellini, 2002) or constant wall temperature (Yardimci *et al.*, 1997; Ramanath *et al.*, 2008; Bellini, 2002) and numerically with FEA (Ramanath *et al.*, 2008; Mostafa *et al.*, 2009; Ji and Zhou, 2010; Bellini *et al.*, 2004). All these analyses assumed perfect contact between the feed filament and the walls of the liquifier. Understanding the impact of any gap between the filament and liquifier walls during heating will provide guidance to the impact of filament diameter tolerances on the performance of the system. Nearly all heat transfer analyses have focused on steady-state operation with a constant feed rate and deposition rate. Of greater interest, especially for the development of advanced control algorithms, are transients in the heat transfer rate that occur when the feed rate is changed. These transients will have a major impact on road-to-road bonding and have only

minimally been addressed in the literature. The presence of these transients also presents an opportunity for exploring the system design, particularly with regard to the heating strategy. Different heating strategies, such as zoned heating, might provide a means of more precisely controlling the temperature. Typically, only a single thermocouple is placed in the liquifier assembly for process control. Experimental measurements at different locations in the liquifier could aid in modeling and process control.

Models of the pressure drop in the liquefier have been drawn from those for extrusion dies. While there has been no reported experimental evaluation of these models in an AM system, they should provide a good quantitative estimate of the pressure drop. Of particular interest is the nature of the flow as the liquifier chamber converges to the nozzle opening. While limits on the convergence angle have been suggested for filled feedstocks to prevent clogging of the nozzle (Yardimci *et al.*, 1997), there have not been any reports of an empirical evaluation of this design limit. Likewise, alignment of polymer chains as they pass through the nozzle opening can be expected to have a significant impact on the mechanical properties of a finished part. This would reasonably be expected to be impacted by the nozzle convergence angle, although a study of this phenomenon in AM systems has not been reported.

Bead spreading and road-to-road bonding determine the surface and mechanical properties of parts made with extrusion AM processes. The ultimate shape of the printed road depends on its surface tension, viscosity, rate of cooling and interaction with the print head. Analytical models of bead spreading should be able to draw from a large body of literature on the spreading of individual droplets on a surface. One such model has been reported (Crockett, 1997; Crockett and Calvert, 1996); however, its assumption of complete wetting without accounting for any change in viscosity with time limits its quantitative value. This model does, however, provide a useful framework for model development. The thermal history of the printed road is of great importance, as it is the greatest determining factor in bonding quality between neighboring roads of material. Simple models provide good qualitative descriptions of the thermal history of a given road. Assumptions made about convective cooling of the printed road do not seem to be justified by any experimental or theoretical basis. Ideally, predictions of thermal history could be related to mechanical bond strength and incorporated into toolpath design algorithms.

Fused deposition modeling® and similar processes are seeing increasing use in finished part manufacturing. Key elements of a typical extrusion-based AM process have been described, and approaches and challenges to modeling each have been reviewed. Continued growth into new markets will require improved understanding of the processing science, enabling development of advanced new materials, model-based process control algorithms and product design rules.

References

Agarwala, M.K., Jamalabad, V.R., Langrana, N.A., Safari, A., Whalen, P.J. and Danforth, S.C. (1996), "Structural quality of parts processed by fused deposition", *Rapid Prototyping Journal*, Vol. 2, pp. 4-19.

Ahn, S.H., Montero, M., Odell, D., Roundy, S. and Wright, P.K. (2002), "Anisotropic material properties of fused deposition modeling ABS", *Rapid Prototyping Journal*, Vol. 8, pp. 248-257.

Bellehumeur, C., Li, L., Sun, Q. and Gu, P. (2004), "Modeling of bond formation between polymer filaments in the fused deposition modeling process", *Journal of Manufacturing Processes*, Vol. 6, pp. 170-178.

Bellini, A. (2002), "Fused deposition of ceramics: a comprehensive experimental, analytical and computational study of material behavior, fabrication process and equipment design", PhD dissertation, Drexel University, Philadelphia, PA.

Bellini, A. and Guceri, S. (2003), "Mechanical characterization of parts fabricated using fused deposition modeling", *Rapid Prototyping Journal*, Vol. 9, pp. 252-264.

Bellini, A., Güçeri, S. and Bertoldi, M. (2004), "Liquefier dynamics in fused deposition", *Journal of Manufacturing Science and Engineering, Transactions of the ASME*, Vol. 126, pp. 237-246.

Bourell, D.L., Leu, M.C. and Rosen, D.W. (Eds) (2009), *Roadmap for Additive Manufacturing: Identifying the Future of Freeform Processing*, The University of Texas at Austin Laboratory for Freeform Fabrication Advanced Manufacturing Series, Austin, TX.

Crockett, R.S. (1997), "The liquid-to-solid transition in stereodeposition techniques", PhD thesis, University of Arizona.

Crockett, R.S. and Calvert, P.D. (1996), "The liquid-to-solid transition in stereodeposition techniques", in Bourell, D.L., Beaman, J.J., Marcus, H.L., Crawford, R.H. and Barlow, J.W. (Eds), *Solid Freeform Fabrication Proceedings*, University of Texas at Austin, Austin, TX, pp. 257-264.

Duineveld, P.C. (2003), "The stability of ink-jet printed lines of liquid with zero receding contact angle on a homogeneous substrate", *Journal of Fluid Mechanics*, Vol. 477, p. 26.

Frenkel, J. (1945), "Viscous flow of crystalline bodies under the action of surface tension", *Journal of Physics (Moscow)*, Vol. 9, pp. 385-391.

Gibson, I., Rosen, D.W. and Stucker, B. (2010), *Additive Manufacturing Technologies: Rapid Prototyping to Direct Digital Manufacturing*, Springer, New York, NY.

Halidi, S.N.A.M. and Abdullah, J. (2012), "Moisture effects on the ABS used for fused deposition modeling rapid prototyping machine", *IEEE Symposium on Humanities, Science and Engineering Research*, *Kuala Lumpur*, pp. 839-843.

Ji, L.B. and Zhou, T.R. (2010), "Finite element simulation of temperature field in fused deposition modeling", *Manufacturing Science and Engineering*,, Vols. 97/101, pp. 2585-2588.

Jones, R., Haufe, P., Sells, E., Iravani, P., Olliver, V., Palmer, C. and Bowyer, A. (2011), "RepRap - the replicating rapid prototyper", *Robotica*, Vol. 29, pp. 177-191.

Karis, T.E., Dawson, D.J., Davis, C.R., Kono, R.N., Kim, G., Jhon, M.S. and Kim, S.J. (1996), "Rapid

prototyping materials rheology", *Journal of Imaging Science and Technology*, Vol. 40, pp. 147-154.

Liang, J.Z. (1995), "Effect of the die angle on the extrusion swell of rubber compound", *Journal of Materials Processing Technology*, Vol. 52, pp. 207-212.

Liang, J.Z. and Ness, J.N. (1997), "Effect of die angle on flow behaviour for high impact polystyrene melt", *Polymer Testing*, Vol. 16, pp. 403-412.

Liang, J.Z., Chan, J.S.F. and Wong, E.T.T. (2001), "Effects of operation conditions and die angles on the pressure losses in capillary flow of polystyrene melt", *Journal of Materials Processing Technology*, Vol. 114, pp. 118-121.

Lipson, H. and Kurman, M. (2010), "Factory@Home: the emerging economy of personal manufacturing", occasional papers in science and technology policy, US Office of Science and Technology Policy, Washington, DC.

Mao, T., Kuhn, D.C.S. and Tran, H. (1997), "Spread and rebound of liquid droplets upon impact on flat surfaces", *AIChE Journal*, Vol. 43, p. 11.

Michaeli, W. (2003), *Extrusion Dies for Plastics and Rubber: Design and Engineering Computations*, Hanser Verlag, Munchen.

Middleman, S. (1995), *Modeling Axisymmetric Flows Dynamics of Films, Jets, and Drops*, Academic Press, San Diego, CA.

Mostafa, N., Syed, H.M., Igor, S. and Andrew, G. (2009), "A study of melt flow analysis of an ABS-iron composite in fused deposition modelling process", *Tsinghua Science and Technology*, Vol. 14, pp. 29-37.

Namii (2012), "Namii website", available at: http://namii.org/ (accessed 28 December 2012).

Osswald, T.A. and Menges, G. (2003), *Materials Science of Polymers for Engineers*, Carl Hanser Verlag, Kempten.

Park, H., Carr, W.W., Zhu, J. and Morris, J.F. (2003), "Single drop impaction on a solid surface", *AIChE Journal*, Vol. 49, p. 11.

Ramanath, H.S., Chua, C.K., Leong, K.F. and Shah, K.D. (2008), "Melt flow behaviour of poly-epsilon-caprolactone in fused deposition modeling", *Journal of Materials Science-Materials in Medicine*, Vol. 19, pp. 2541-2550.

Rosenzweig, N. and Narkis, M. (1981), "Sintering rheology of amorphous polymers", *Polymer Engineering and Science*, Vol. 21, pp. 1167-1170.

Scott, J., Gupta, N., Weber, C., Newsome, S., Wohlers, T. and Caffrey, T. (2012), *Additive Manufacturing: Status and Opportunities*, Institute for Defense Analysis: Science and Technology Policy Institute, Washington, DC.

Shofner, M.L., Lozano, K., Rodríguez-Macías, F.J. and Barrera, E.V. (2003), "Nanofiber-reinforced polymers prepared by fused deposition modeling", *Journal of Applied Polymer Science*, Vol. 89, pp. 3081-3090.

Sun, Q., Rizvi, G.M., Bellehumeur, C.T. and Gu, P. (2008), "Effect of processing conditions on the bonding quality of FDM polymer filaments", *Rapid Prototyping Journal*, Vol. 14, pp. 72-80.

Thomas, J.P. and Rodriguez, J.F. (2000), "Modeling the fracture strength between fused deposition extruded roads", *Solid freeform Fabrication Proceedings*, University of Texas at Austin, Austin, TX, pp. 16-23.

Venkataraman, N., Rangarajan, S., Harper, B., Matthewson, M.J., Safari, A. and Danforth, S.C. (2000a), "Process-property-performance relationship for fused deposition of ceramics (FDC) feedstock materials", in Danforth, S.C., DIMOS, D. and Prinz, F.B. (Eds), *Solid Freeform and Additive Fabrication*, San Francisco, CA, pp. 203-210.

Venkataraman, N., Rangarajan, S., Matthewson, M.J., Harper, B., Safari, A., Danforth, S.C., Wu, G., Langrana, N., Guceri, S. and Yardimci, A. (2000b), "Feedstock material property-process relationships in fused deposition of ceramics (FDC)", *Rapid Prototyping Journal*, Vol. 6, pp. 244-252.

Venkataraman, N., Rangarajan, S., Matthewson, M.J., Safari, A., Danforth, S.C. and Yardimci, A. (1999), "Mechanical and rheological properties of feedstock material for fused deposition of ceramics and metals (FDC and FDMet) and their relationship to process performance", in Bourell, D.L., Beaman, J.J., Crawford, R.H., Marcus, H.L. and Barlow, J.W. (Eds), *Solid Freeform Fabrication Proceedings*, University of Texas at Austin, Austin, TX.

Wang, T.M., Xi, J.T. and Jin, Y. (2007), "A model research for prototype warp deformation in the FDM process", *International Journal of Advanced Manufacturing Technology*, Vol. 33, pp. 1087-1096.

Wohlers, T.T. (2011), *Wohlers Report 2011: Additive Manufacturing and 3D Printing State of the Industry Annual Worldwide Progress Report*, Wohlers Associates, Inc., Fort Collins, CO.

Yardimci, M.A., Hattori, T., Guceri, S.I. and Danforth, S.C. (1997), "Thermal analysis of fused deposition", in Bourell, D.L., Beaman, J.J., Crawford, R.H., Marcus, H.L. and Barlow, J.W. (Eds), *Solid Freeform Fabrication Proceedings*, University of Texas at Austin, Austin, TX.

About the authors

Brian N. Turner is a Post-doctoral Research Associate at the University of Dayton. He received his undergraduate degree from that institution in Chemistry before completing his PhD in Chemistry at Vanderbilt University.

Robert Strong will complete his BS in Chemical Engineering at the University of Dayton in the spring of 2013, where he subsequently plans to earn his MS in the same discipline.

Scott A. Gold has been an Associate Professor in the Chemical and Materials Engineering Department at the University of Dayton since 2010. Prior to that, he was on the faculty at Louisiana Tech University. He served as a Post-doctoral researcher at the University of Illinois-Urbana Champaign and earned his PhD in Chemical Engineering from Arizona State University. Scott Gold is the corresponding author and can be contacted at: sgold1@udayton.edu

To purchase reprints of this article please e-mail: **reprints@emeraldinsight.com**
Or visit our web site for further details: **www.emeraldinsight.com/reprints**